The Role of Carrier Transport on the Current Injection Efficiency of InGaAsN Quantum-Well Lasers

Jeng-Ya Yeh, Luke J. Mawst, and Nelson Tansu

***Abstract*—A theoretical and experimental study demonstrates that the current injection efficiency of InGaAsN quantum-well (QW) lasers can be significantly affected by carrier transport in the separate confinement heterostructure (SCH) region. An offset QW design is utilized to show the impact of hole transport on the temperature dependence of the external differential quantum efficiency and above threshold injection efficiency. A reduction of the current injection efficiency is found for structures which have significant hole transport times in the SCH.**

***Index Terms*—Current injection efficiency, InGaAsN, long wavelength quantum-well (QW) laser, material gain, temperature sensitivity, thermionic carrier leakage.**

I. Introduction

The CURRENT injection efficiency $\eta_{\rm inj}$ of quantum-well (QW) lasers, defined as the fraction of injected current or carriers which recombines (both radiatively and nonradiatively) in the QW, has a direct impact on both threshold current density and external differential quantum efficiency. Furthermore, the temperature dependence of $\eta_{\rm inj}$ can be significant in some laser structures, leading to a high temperature sensitivity of both threshold current and external differential quantum efficiency. Improved understanding of the mechanisms impacting $\eta_{\rm inj}$ provides a key to further optimize devices for efficient high output power and high temperature operation. Recent studies have indicated that $\eta_{\rm inj}(T)$ plays a significant role in the observed strong temperature dependence of 1.3-μm InGaAsN single QW lasers [1]. Here we report results of a theoretical and experimental study on the impact of carrier transport on $\eta_{\rm inj}$ for InGaAsN QW lasers, providing insight into the design optimization of these laser structures.

In order to examine the effects of carrier transport on $\eta_{\rm inj}$, a laser structure design consisting of an asymmetrically placed QW was utilized. In this experiment, we focused on two laser structures for which the active region is intentionally placed close to either the p-cladding or n-cladding layers. This method was also utilized by Nagarajan *et al.* to demonstrate the impact of QW position on device high-frequency modulation response performance [2]. With this design, we altered the scenario of carrier transport but fixed the threshold gain condition between these two lasers (i.e., same optical confinement factor Γ, mirror loss α_m, and internal loss α_i), resulting in nominally identical values of threshold carrier density $N_{\rm th}$. Therefore, identical recombination lifetime and thermionic escape lifetime of carriers in the QW are expected. This allows us to study directly the carrier transport effects on the device $\eta_{\rm inj}$ without consideration of carrier recombination and leakage processes. The effect of carrier transport was analyzed using a theoretical model and good agreement with experiment was found.

Manuscript received December 6, 2004; revised February 28, 2005.

J.-Y. Yeh and L. J. Mawst are with the Reed Center for Photonics, Department of Electrical and Computer Engineering, University of Wisconsin-Madison, Madison, WI 53706-1691 USA (e-mail: jyeh@cae.wisc.edu).

N. Tansu is with the Center for Optical Technologies, Department of Electrical and Computer Engineering, Lehigh University, Bethlehem, PA 18015 USA.

Digital Object Identifier 10.1109/LPT.2005.852331

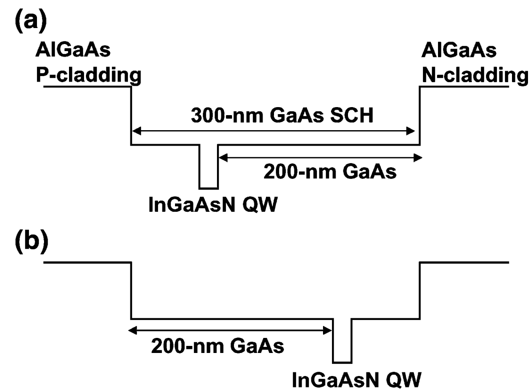

Fig. 1. Schematic band diagram of the offset QW structures. The active region is closer to (a) p-cladding for Laser P and (b) n-cladding for Laser N.

II. Laser Structure Design and Lasing Characteristics

The laser materials were grown by low-pressure metal–organic vapor deposition with sources of trimethylgallium, trimethylaluminum, trimethylindium, AsH_3, PH_3, and dimethylhydrazine. The InGaAsN QW is located a distance 100 nm from the p-type cladding layer for Laser P, and 100 nm from the n-type cladding layer for Laser N while keeping the thickness of the GaAs separate confinement heterostructure (SCH) 300 nm for both structures. Fig. 1 shows the schematic energy band diagrams of both Lasers P and N. Not shown in Fig. 1 for simplicity, are 10-nm GaAs setback layers and 7.5-nm $GaAs_{0.85}P_{0.15}$ strain compensation layers surrounding the 8-nm $In_{0.4}Ga_{0.6}As_{0.995}N_{0.005}$ QW, as discussed in [3]. The 1.1-μm-thick p-type and n-type AlGaAs cladding layers have a doping level of 1×10^{18} cm^{-3} and the GaAs SCH region is undoped. The lasing characteristics were studied under pulse condition with a 1% duty cycle for broad area devices with 100-μm-wide stripes. The lasing wavelength is 1.29 μm at room temperature. Fig. 2 shows the measured threshold current density $(J_{\rm th})$ and external differential quantum efficiency (η_d) versus heat sink temperature for Lasers P and N, both with 2-mm-long cavity lengths. At 20 °C, $J_{\rm th}$ is 249 A/cm^2 and η_d is 31.7% for Laser N, and improved to 207 A/cm^2 and 33.4% for Laser P. Both lasers share a similar T_0 $(1/T_0 = 1/J_{\rm th} \times (dJ_{\rm th}/dT))$ value around 100 K, but

1041-1135/$20.00 © 2005 IEEE

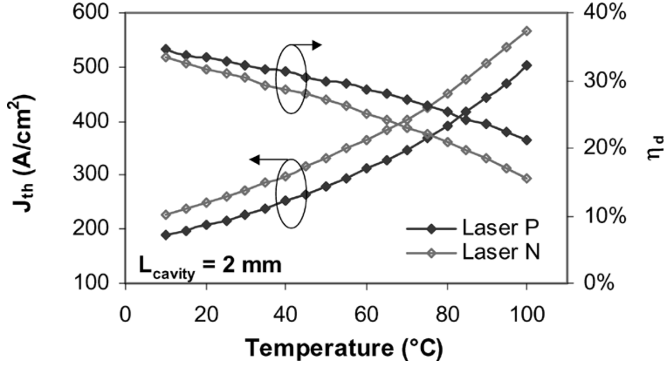

Fig. 2. Measured temperature dependence of threshold current density and external differential quantum efficiency of Lasers P and N. Laser P has a smaller J_{th} and higher η_d.

Laser P has an improved T_1 $(1/T_1 = -1/\eta_d \times (d\eta_d/dT))$ value of 270 K compared to 175 K for Laser N.

III. Current Injection Efficiency Model and Experimental Results

The current injection efficiency for InGaAsN QW lasers has been analyzed theoretically [4]. By using the steady-state two level rate equations considering carriers in the QW and barrier/SCH regions, the below-threshold $(\eta_{\text{inj_below_th}})$ and above-threshold $(\eta_{\text{inj_above_th}})$ current injection efficiency can be derived as follows [4]:

$$\eta_{\text{inj_below_th}} = \frac{1}{1+\frac{\tau_{\text{bw}}}{\tau_b}\cdot\left(1+\frac{\tau_{\text{QW_total}}}{\tau_{\text{esc}}}\right)} \tag{1}$$

$$\eta_{\text{inj_above_th}} = \eta_{\text{structure}} \cdot \frac{1-\Delta_{\text{QW}}\cdot\left[\frac{1}{\eta_{\text{inj_below_th}}}-\beta\cdot\left(1+\frac{\tau_{\text{bw}}}{\tau_b}\right)\right]}{1+\frac{\tau_{\text{bw}}}{\tau_b}}. \tag{2}$$

In these two equations, $\eta_{\text{inj_below_th}}$ and $\eta_{\text{inj_above_th}}$ are described by the lifetimes associated with the four dominant processes, including carrier radiative and nonradiative recombination in the QW $(\tau_{\text{QW_total}})$ and SCH (τ_b), ambipolar carrier transport in the SCH (τ_{bw}) [5], and thermionic leakage of carriers escaping out of the QW (τ_{esc}) [6]. In this model, the carrier capture time is not included due to its smaller value (around one order of magnitude) compared to the transport time τ_{bw} [7]. In (2), $\eta_{\text{structure}}$, Δ_{QW}, and β represent the current injection efficiency from cladding region to SCH (i.e., structure dependent), the above threshold carrier unclamping rate, and spontaneous emission factor, respectively. In the ideal condition, N_{QW} remains pinned at and above laser threshold. In reality, N_{QW} may not be fully clamped and the carrier unclamping rate Δ_{QW} is defined as the rate of increase of carriers in the QW due to an increase in the injection current, for the above threshold condition. It can be expressed as $\Delta(N_{\text{QW}} \times V_{\text{QW}}/\tau_{\text{QW_total}})/\Delta(I_{\text{SCH}}/q)$, where N_{QW}, V_{QW}, and I_{SCH} are the carrier density in the QW, volume of the QW, and injection current from the cladding layers [4]. In this study, $\eta_{\text{structure}}$ and Δ_{QW} were chosen to be 85% and 15%, respectively, and assumed temperature independent. The less than unity $\eta_{\text{structure}}$ in the laser structure is typically resulted from the defect recombination at the poor interfaces in the cladding-SCH interface, leading to a reduction of the $\eta_{\text{structure}}$.

A careful examination for the carrier lifetimes of these four major processes is necessary. Details of τ_{esc} and the modeling method used here are extensively discussed in [1] and [4]. To evaluate $\tau_{\text{QW_total}}$, a knowledge of the monomolecular, bimolecular, and Auger recombination coefficients A, B, and C, and their temperature dependence, are crucial. However, based on our calculation, we find that $\tau_{\text{QW_total}}$ has little effect on the calculated η_{inj} mainly due to a much higher temperature sensitivity of τ_{esc} for the structures under study. In our simulation, we utilized the published values of A, B, and C parameters in [8]. The carrier transport behavior in the SCH obeys the ambipolar carrier transport and can be expressed by the equation as follows:

$$\tau_{\text{bw}} = \frac{1}{2}\cdot\left(\frac{L_n^2}{2\cdot D_n}+\frac{L_p^2}{2\cdot D_p}\right) \tag{3}$$

where L_n and L_p are the thickness of GaAs SCH measured from the QW edge to n-cladding and p-cladding, respectively. The D_n and D_p are the diffusion coefficients of electrons and holes, respectively, which can be related to carrier mobility by the Einstein relation. Since the undoped GaAs SCH is background n-type ($n \sim 10^{16}$ cm^{-3}), the majority electron mobility and minority hole mobility were used in this calculation. Due to the significantly smaller value of hole mobility μ_p ($\sim$400 cm^2/Vs at 300 K) compared to electron mobility μ_n ($\sim$9200 cm^2/Vs) [9], τ_{bw} is ultimately determined by how fast holes can move across SCH region to QW and electron transport has a minimal effect. The significance of the temperature dependence of the minority hole mobility on η_{inj} should also be noted. In our model, we utilized a $1/T$ relationship for μ_p, as observed by Lovejoy *et al.* [10], which results in a temperature-independent D_p. Therefore, τ_{bw} only slightly increases with temperature, which is attributed to D_n. Our calculations yield a smaller τ_{bw} value of about $3 - 3.3 \times 10^{-12}$ s for Laser P compared to $9.82 - 9.88 \times 10^{-12}$ s for Laser N, indicating the effect of the offset QW position. For calculating τ_b, we utilized the following equations, considering carrier recombination in the QW, thermionic escape rate, and carrier transport in the SCH [4]:

$$N_B = N_{\text{QW}}\cdot\left(\frac{1}{\tau_{\text{QW_Total}}}+\frac{1}{\tau_{\text{esc}}}\right)\cdot\left(\frac{V_{\text{QW}}}{V_B}\right)\cdot\tau_{\text{bw}} \tag{4}$$

$$\tau_b = \frac{1}{A_B + B_B\cdot N_B} \tag{5}$$

where N_B, A_B, B_B are the carrier density, monomolecular, and bimolecular recombination coefficients in the SCH and V_B is the volume of the SCH. The calculated τ_b of Lasers P and N both exhibit a monotonically decreasing behavior with temperature, reducing from 9.5×10^{-9} s at 10 °C to 8.2×10^{-9} s at 100 °C for Laser P and from 8.6×10^{-9} s at 10 °C to 6.1×10^{-9} s at 100 °C for Laser N. The longer τ_b for Laser P arises from its smaller τ_{bw} value compared to Laser N. Moreover, stronger carrier leakage at high temperature leads to an increased N_B and, therefore, a reduced τ_b.

To compare the experimental results with the model, $\eta_{\text{inj_above_th}}$ can be extracted experimentally by performing a conventional cavity length analysis [11]. Fig. 3 shows measured $\eta_{\text{inj_above_th}}$ as a function of temperature for the two laser structures, as well as the calculated values from the analysis

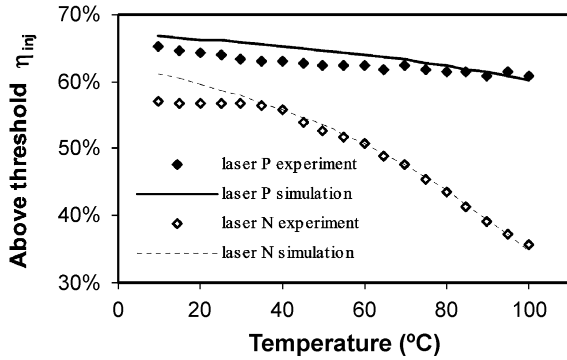

Fig. 3. Measured and calculated current injection efficiency above threshold as function of temperature.

(2). Useful insights can be obtained by measuring the temperature dependence of $\eta_{\rm inj_above_th}$ and defining a characteristic temperature coefficient $(T_{\eta {\rm inj_above_threshold}})$ [12]. Shown in Fig. 3 are the measured characteristic temperature coefficient values of $\eta_{\rm inj_above_th}$ (i.e., $T_{\eta {\rm inj_above_threshold}}$), with values 1400 K and 190 K for Lasers P and N, respectively. With a shorter distance for holes to travel, Laser P not only exhibits an improved $\eta_{\rm inj_above_th}$ compared with that of Laser N, but also a very high characteristic temperature, indicating low temperature sensitivity. The large difference of the temperature dependence of $\eta_{\rm inj_above_th}$ for Lasers P and N can be attributed to the importance of the carrier transport behavior. Comparing the data shown in Fig. 3, although deviation in the lower temperature region occurs, this model accurately predicts the temperature dependence of the above threshold injection efficiency for the structures with an offset QW. Furthermore, the consistency between the experimental and calculated results validates this analytical model.

The high value of $T_{\eta {\rm inj_above_threshold}}$ of Laser P does not necessarily lead to an equally high T_1 value (i.e., $T_1 = 175$ K for Laser N and 270 K for Laser P). This can be understood from the fact that, for Laser P, the dominant factor influencing the T_1 value is not $T_{\eta {\rm inj}}$ but $T_{\alpha i}$, the characteristic temperature coefficient of the internal loss α_i. According to the temperature sensitivity analysis given in [12], T_1 can be expressed in terms of $T_{\eta {\rm inj_above_threshold}}$ and $T_{\alpha i}$

$$\frac{1}{T_1(L)} = \frac{1}{T_{\eta {\rm inj_above_threshold}}} + \frac{\alpha i}{\alpha i + \alpha m(L)} \cdot \frac{1}{T_{\alpha i}} \quad (6)$$

where the mirror loss $\alpha_m(L) = (1/L) \times \ln(1/R)$ is a function of cavity length L and reflectivity R. Extracted from a temperature-dependent cavity length analysis, $T_{\alpha i}$ of Laser P is found to be only 189 K. As a result, $T_{\alpha i}$ limits the temperature dependence of the laser efficiency (i.e., limits T_1) for Laser P, regardless of the extremely high $T_{\eta {\rm inj_above_threshold}}$ value of 1400 K. In addition, the much lower $J_{\rm th}$ value observed for Laser P originates from the higher $\eta_{\rm inj_below_th}$. From (1), the room temperature $\eta_{\rm inj_below_th}$ and its characteristic temperature coefficient were calculated to be 86% and 300 K for Laser P, and 64% and 120 K for Laser N. Thus, for Laser N, the 20% reduction of $\eta_{\rm inj_below_th}$ and lower g_{oJ} compared to Laser P leads to the observed increase in $J_{\rm th}$.

It is also necessary to emphasize the crucial role of carrier leakage in this experiment. According to (1) and (2), the impact of carrier transport on $\eta_{\rm inj}$ strongly depends on the competition between $\tau_{\rm esc}$ and $\tau_{\rm bw}$. For the InGaAsN QW structure, due to the process of hole thermionic escape, $\tau_{\rm esc}$ is estimated to be on the order of 10^{-12} s. On the other hand, τ_e is estimated to be 10^{-11} s for an InGaAs QW with the same SCH structure [1]. Having a much longer $\tau_{\rm esc}$, the impact of adjusting the InGaAs QW position to reduce the effective $\tau_{\rm bw}$ is not as significant as the case of the InGaAsN QW laser, and the model indicates that an almost indistinguishable $\eta_{\rm inj_above_th}$ would result over a wide temperature range for an InGaAs QW. As a result, locating the QW close to p-type cladding layer does not necessarily lead to an improved $\eta_{\rm inj}$, unless $\tau_{\rm esc}$ is small enough so that the change of $\tau_{\rm bw}$ is relatively pronounced.

IV. Conclusion

Two InGaAsN QW lasers with asymmetrically placed active region were carefully studied and compared. The experimental results were well predicted and explained by an analytical injection efficiency model. Improved $J_{\rm th}$, η_d, and $\eta_{\rm inj_above_th}$ for the laser with the InGaAsN QW close to p-side indicates the importance of optimizing the QW location. The model allows for an improved understanding of the mechanisms of the carrier transport and injection efficiency of the diode laser, which is essential to achieving higher device performance.

References

[1] N. Tansu and L. J. Mawst, "The role of hole leakage in 1300-nm InGaAsN quantum-well lasers," *Appl. Phys. Lett.*, vol. 82, no. 10, pp. 1500–1502, Mar. 2003.
[2] R. Nagarajan, R. P. Mirin, T. E. Reynolds, and J. E. Bowers, "Experimental-evidence for hole transport limited intensity modulation response in quantum-well lasers," *Electron. Lett.*, vol. 29, no. 19, pp. 1688–1690, Sep. 1993.
[3] N. Tansu, N. J. Kirsch, and L. J. Mawst, "Low-threshold-current-density 1300-nm dilute-nitride quantum well lasers," *Appl. Phys. Lett.*, vol. 81, no. 14, pp. 2523–2525, Sep. 2002.
[4] N. Tansu and L. J. Mawst, "Current injection efficiency of InGaAsN quantum-well lasers," *J. Appl. Phys.*, vol. 97, p. 054 502, Mar. 2005.
[5] R. Nagarajan, M. Ishikawa, T. Fukushima, R. S. Geels, and J. E. Bowers, "High-speed quantum-well lasers and carrier transport effects," *IEEE J. Quantum Electron.*, vol. 28, no. 10, pp. 1990–2008, Oct. 1992.
[6] H. Schneider and K. V. Klitzing, "Thermionic emission and Gaussian transport of holes in a GaAs/AlGaAs multiple-quantum-well structure," *Phys. Rev. B*, vol. 38, no. 9, pp. 6160–6165, Sep. 15, 1988.
[7] H. Hirayama, J. Yoshida, Y. Miyake, and M. Asada, "Carrier capture time and its effects on the efficiency of quantum-well lasers," *IEEE J. Quantum Electron.*, vol. 30, no. 1, pp. 54–62, Jan. 1994.
[8] R. Fehse, S. Tomic, A. R. Adams, S. J. Sweeney, E. P. O'Reilly, A. Andreev, and H. Riechert, "A quantitative study of radiative, Auger, and defect related recombination processes in 1.3-mu m GaInNAs-based quantum-well lasers," *IEEE J. Sel. Topics Quantum Electron.*, vol. 8, no. 4, pp. 801–810, Jul. 2002.
[9] S. L. Chuang, *Physics of Optoelectronic Devices*. New York: Wiley, 1995.
[10] M. L. Lovejoy, M. R. Melloch, and M. S. Lundstrom, "Temperature-dependence of minority and majority carrier mobilities in degenerately doped gaas," *Appl. Phys. Lett.*, vol. 67, no. 8, pp. 1101–1103, Aug. 1995.
[11] L. A. Coldren and S. W. Corzine, *Diode Lasers and Photonic Integrated Circuits*, 1st ed. New York: Wiley, 1995.
[12] N. Tansu, Y. L. Chang, T. Takeuchi, D. P. Bour, S. W. Corzine, M. R. T. Tan, and L. J. Mawst, "Temperature analysis and characteristics of highly strained InGaAs-GaAsP-GaAs $(\mathrm{lambda} > 1.17\ \mu\mathrm{m})$ quantum-well lasers," *IEEE J. Quantum Electron.*, vol. 38, no. 6, pp. 640–651, Jun. 2002.